

# Stabilization of Electron-Dense Palladium–Hydrido Complexes in Solid-State Hydrides

Malin Olofsson-Mårtensson,<sup>†</sup> Ulrich Häussermann,<sup>‡</sup> John Tomkinson,<sup>§</sup> and Dag Noréus<sup>\*,†</sup>

Contribution from the Department of Structural Chemistry and the Department of Inorganic Chemistry, Stockholm University, S-106 91 Stockholm, Sweden, and Rutherford Appleton Laboratory, Chilton, Didcot, Oxfordshire OX11 0QX, UK

Received November 22, 1999

**Abstract:** Inelastic neutron scattering, supported by IR and Raman spectroscopy, has been used to observe a decreasing Pd–H bond strength in a series of four low-valent palladium–hydrogen complexes in the solid-state hydrides:  $K_2[Pd(II)H_4]$ ,  $Li_2[Pd(0)H_2]$ ,  $Na_2[Pd(0)H_2]$ ,  $NaBa[Pd(0)H_3]$ , and  $Ba_2[Pd(0)H_4]$ . Further, self-consistent linear muffin-tin orbital calculations of the electronic structures describe the palladium–hydrido complexes in a  $sd^n$  hybridization with a decreasing Pd–H bond order as an increasing number of antibonding orbitals must be utilized. A strong support to the bonding from the cations via easily polarizable  $H^-$  is, however, necessary to explain the stability of the systems. The effect of the large polarizability of hydrogen can in this respect be compared with the more conventional “back-bonding” to ligand orbitals for stabilizing a formal low-valent oxidation state by distributing electron density away from the central atom.

## Introduction

By reacting electropositive alkali and alkaline earth metals (s-metals) with group VII, VIII, IX, and X transition metals (TM) in the presence of hydrogen a large number of ternary and quaternary metal hydrides based on TM–hydrido complexes have been synthesized in the last 20 years. In their synthesis the s-elements are supplying their valence electrons to allow for the formation of usually 18-electron but also 16-electron homoleptic TM–hydrido complexes. Two 14-electron and possibly a 17-electron complex have also been proposed.<sup>1,2</sup> Some of the hydrides have in addition to the TM–hydrido complexes, hydrogen bound in interstitial sites coordinated by the s-elements forming structural building blocks similar to the structures of the binary alkali and alkaline earth hydrides. The puzzling variety of compositions, transition metal coordinations, and geometries have generated a number of theoretical studies.<sup>3–7</sup> Very recently two rather contradictory concepts were presented in this journal trying to rationalize mainly the coordination geometries and electron counts in the new hydrido complexes. Firman and Landis propose a Valence Bond (VB) model with  $sd^n$  hybridized transition metal orbitals leading to hypervalently bonded hydrido complexes for systems with more than 12 valence electrons.<sup>3</sup> Bayse and Hall claim the necessity of the inclusion of transition metal  $(n+1)p$  orbitals for a correct bonding description, which they assume to be based on two-center, two-electron electron ligand bonding.<sup>4</sup>

Among the new hydrides an increasing number of solid-state hydrides based on  $d^{10}$  formal low valent transition metal–hydrido complexes have been synthesized. The family now comprises the members  $Li_2(PdH_2)$ ,  $Na_2(PdH_2)$ ,  $NaBa(PdH_3)$ ,  $Sr_2(PdH_4)$ ,  $Ba_2(PdH_4)$ ,  $Mg_2(NiH_4)$ , and  $Mg_3(RuH_3)$ .<sup>8–13</sup> Also these hydrides can be made fairly conveniently by hot sintering in hydrogen of compacted powder mixtures of the binary alkali or alkaline earth hydrides with the corresponding transition metal. The existence of these complexes is interesting as such low formal valent oxidation states of the transition metal are usually associated with ligands having good electron-accepting properties. This conventional stabilization by “back-donation” to ligand orbitals is, however, not available in homoleptic hydrido complexes.

Some of the hydrides show metallic electric conductivity, indicating that the cations are required to participate more in the bonding, beyond the role of a conventional undeformed cation. Thus it seems likely that a stabilization mechanism for these electron dense low formal oxidation states is to be found in the interaction of the hydrogen ligands with the cations surrounding the complexes. This could correspond to a somewhat indirect “back-bonding” mechanism where electron density from the d-orbitals of the transition metals are distributed to the cations via bonding with the hydrogen atoms. Such a mechanism could also be of interest for application as it may offer a way to influence the stability of a complex and thus the hydrogen release pressure by manipulating the “electropositive matrix” surrounding the complexes.

\* Address correspondence to this author.

<sup>†</sup> Department of Structural Chemistry, Stockholm University.

<sup>‡</sup> Department of Inorganic Chemistry, Stockholm University.

<sup>§</sup> Rutherford Appleton Laboratory.

(1) Yvon, K. *Chimia* 1998, 52, 613.

(2) Bronger, W. *Angew. Chem., Int. Ed. Engl.* 1991, 30, 759.

(3) Firman, T. K.; Landis, C. R. *J. Am. Chem. Soc.* 1998, 120, 12650.

(4) Bayse, C. A.; Hall, M. B. *J. Am. Chem. Soc.* 1999, 121, 1348.

(5) King, R. B. *Inorg. Chem.* 1998, 37, 3057.

(6) Miller, G. J.; Deng, H.; Hoffmann, R. *Inorg. Chem.* 1994, 33, 1330.

(7) Liao, M.-S.; Zhang, Q.-R.; Schwarz, W. H. E. *Z. Anorg. Allg. Chem.* 1998, 624, 1419.

(8) Kadir, K.; Noréus, D. *Z. Phys. Chem. N.F.* 1989, 163, 231.

(9) Noréus, D.; Törnroos, K. W.; Börje, A.; Szabó, T.; Bronger, W.; Spittank, H.; Auffermann, G.; Müller, P. *J. Less Common Met.* 1988, 139, 233.

(10) Olofsson, M.; Kritikos, M.; Noréus, D. *Inorg. Chem.* 1998, 37, 2900.

(11) Olofsson-Mårtensson, M.; Kritikos, M.; Noréus, D. *J. Am. Chem. Soc.* 1999, 121, 10908.

(12) Zolliker, P.; Yvon, K.; Jorgensen, D.; Rotella, F. J. *Inorg. Chem.* 1986, 25, 5, 3590.

(13) Bonhomme, F.; Yvon, K.; Fischer, P. *J. Alloys Compd.* 1992, 186, 309.

In the present paper we want to further investigate the importance of this interaction with the cations on the stability of the complexes by investigating the bond strength of the metal–hydrogen in the series  $K_2(\text{Pd}(\text{II})\text{H}_4)$ ,  $\text{Li}_2(\text{Pd}(\text{0})\text{H}_2)$ ,  $\text{Na}_2(\text{Pd}(\text{0})\text{H}_2)$ ,  $\text{NaBa}(\text{Pd}(\text{0})\text{H}_3)$ , and  $\text{Ba}_2(\text{Pd}(\text{0})\text{H}_4)$ .

IR, Raman, and inelastic neutron scattering spectroscopy were combined with self-consistent electron band structure calculations to better understand and interpret the systems. Hopefully the experience gained from these special systems will contribute to a more general understanding of new complex metal hydride systems.

## Experimental Section

**Synthesis and Structure Determinations.**  $K_2\text{PdH}_4$ ,  $\text{Li}_2\text{PdH}_2$ ,  $\text{Na}_2\text{PdH}_2$ ,  $\text{NaBaPdH}_3$  and  $\text{Ba}_2\text{PdH}_4$  were all synthesized by direct reaction between hydrogen and the nominal compositions of the alkaline and/or alkaline earth metal hydrides and palladium under conditions described previously.<sup>7–10,14</sup> All samples are air and moisture sensitive and were therefore handled and stored under argon atmosphere. The structures have already been determined using single-crystal X-ray diffraction or powder X-ray diffraction of the hydrides combined with neutron powder diffraction on the corresponding deuterides to locate the hydrogen atoms.<sup>7–10,14</sup> Phase analysis on all samples in this investigation was performed by powder X-ray diffraction using a focusing Guiner–Hägg camera and the samples were found to be single phased.

**Infrared and Raman Spectroscopy.** Mid-infrared spectra of  $K_2\text{PdH}_4$  and  $\text{NaBaPdH}_3$  were recorded on KBr disks with a Bruker IFS 55 spectrometer. The Raman spectrum of  $K_2\text{PdH}_4$  was recorded with a Renishaw Raman system 1000 spectrometer equipped with a Leica microscope and a 782 nm excitation from a diode laser with the hydride powder in a sealed glass capillary.

**Inelastic Neutron Scattering (INS) Spectroscopy.** The INS data were recorded at  $\sim 20$  K at the pulsed neutron source at ISIS, Rutherford Appleton Laboratory in Chilton, U.K. using the high-resolution broadband spectrometer TFXA.<sup>15</sup> The spectrometer has an inverted time-of-flight geometry and the sample, a sealed aluminum can containing 5–10 g of the hydride, is illuminated by pulsed, polychromatic neutrons. Only the neutrons backscattered by an angle of  $135^\circ$  and having a energy of  $32\text{ cm}^{-1}$  (4.12 meV) are Bragg scattered by the pyrolytic graphite analyzer crystal and reach the  $\text{He}^3$  detector bank.

The intensity of the  $i$ th INS band at an energy transfer of  $\omega_i$  is given by

$$S(Q, \omega_i) \propto \sigma Q^2 U_i^2 \exp(-Q^2 U_T^2) \quad (1)$$

where  $Q$  is the momentum transfer ( $\text{\AA}^{-1}$ ),  $\omega$  is the energy transfer ( $\text{cm}^{-1}$ ),  $\sigma$  is the total scattering cross section,  $U_i^2$  is the mean square displacement of the atoms contributing to the  $i$  mode, and  $U_T^2$  is the total mean-squared displacement. Since hydrogen is both the lightest atom and has the largest total scattering cross section of 82.02 barns compared to Li (1.37 barns), Na (3.28 barns), Ba (3.38 barns), and Pd (4.48 barns) and since the intensity is dependent both on the amplitude of vibration ( $U_i^2$ ) and on the cross section ( $\sigma$ ), the hydrogen motions will dominate the spectra.

The spectrometer TFXA is designed so each value on the energy transfer  $\omega$  corresponds to a fixed value of the momentum transfer  $Q$  ( $\omega \approx 2Q^2$ ). The spectral resolution is 2% of the energy transfer between 16 and  $4000\text{ cm}^{-1}$  and the spectra can be divided into different parts: first the elastic peak at  $E_{\text{transfer}} = 0\text{ cm}^{-1}$ , then the external modes (phonon, translation, and librations) and at higher energies the internal modes (deformation and stretches). The INS spectra also show features as overtones and combination bands between different internal modes. If the molecule (complex) is affected by the lattice vibration combina-

tion bands between the external and internal modes, so-called phonon wings are observed. These can severely complicate the interpretation of the spectra, but fortunately for this work the palladium complexes can be considered as fairly heavy which reduces the effect. The most important feature of INS spectroscopy, compared to IR and Raman spectroscopy, is that *all* modes are allowed, including optical and acoustic modes.

**CLIMAX Refinements.** The program CLIMAX includes a normal coordinate analysis based on the experimental intensities and frequencies. It is developed to fit and minimize a force field to an INS spectrum, calculating both energy and intensities from the eigenvalues and eigenvectors obtained in the normal coordinate analysis. The atomic position in the palladium complexes used as input was taken from our previous structural determinations including the counterions with the closest distance to the hydrogen atoms, to partially account for the influence of the lattice. This also made it possible to calculate the intensities of the librational modes, which in the INS spectra are very strong and therefore have a large impact on the spectra at higher energy from their overtones and combination bands.

To reduce the number of parameters the molecular point group symmetry of the complexes is used. The force field is fitted to the whole spectral profile to determine the force constants as this information is spread over many peaks. A more detailed description of the program is found in papers by Kearley.<sup>16,17</sup>

**Computational Details for the Electronic Structures.** To obtain a more detailed and fuller bonding description, the electronic structures of the compounds  $\text{Na}_2\text{PdH}_2$ ,  $\text{Li}_2\text{PdH}_2$ ,  $\text{Na}_2\text{PdH}_4$ ,  $\text{NaBaPdH}_3$ , and  $\text{Ba}_2\text{PdH}_4$  were calculated self-consistently using the local density-functional approximation and the scalar relativistic linear muffin-tin orbital (LMTO) method in the atomic sphere approximation (ASA) including the combined correction (program TB-LMTO 4.6<sup>18</sup>). The exchange-correlation potential was parametrized according to von Barth and Hedin.<sup>19</sup> The TB-LMTO 4.6 program automatically allows in a procedure the search of empty sphere (ES) positions and the determination of sphere radii.<sup>20</sup> ES had to be introduced for all structures to avoid large overlap for the atomic spheres. Space filling was achieved within the recommended overlap ranges between the different spheres.<sup>21</sup> The basis consisted of Pd s-, p-, d-, and (downfolded) f-LMTOs, H, Li, and Na s- and (downfolded) p- and d-LMTOs, and Ba s-, p-, and (downfolded) d- and f-LMTOs. The reciprocal space integrations were performed with the tetrahedron method<sup>22,23</sup> using 185 ( $\text{Na}_2\text{PdH}_2$ ,  $\text{Li}_2\text{PdH}_2$ ), 33 ( $\text{Na}_2\text{PdH}_4$ ), 28 ( $\text{NaBaPdH}_3$ ), and 45 ( $\text{Ba}_2\text{PdH}_4$ ) irreducible k-points.

## Discussion

**Pd–H Force Constants, INS Spectra, and CLIMAX Refinements.**  $K_2\text{PdH}_4$  is a nonconducting yellow greenish powder that crystallizes in the tetragonal space group  $I4/mmm$  with the unit cell dimensions of  $a = 5.831(1)\text{ \AA}$  and  $c = 7.692(1)\text{ \AA}$ . The structure consists of square-planar,  $D_{4h}$ -symmetry  $[\text{PdH}_4]^{2-}$  units counterbalanced by potassium ions surrounding each complex in a cubic configuration (Figure 1). The distance between the formally divalent palladium and the hydrogen atoms is  $1.625(8)\text{ \AA}$  and the shortest potassium–hydrogen distance is  $2.853(4)\text{ \AA}$ .

From the selection rules for infrared and Raman spectroscopy of a molecule with  $D_{4h}$ -symmetry three vibrations are IR active and three are Raman active: the doubly degenerate stretch ( $E_u$ ), the doubly degenerate deformation ( $E_u$ ), and the symmetric out-

(16) Kearley, G. J. *J. Chem. Soc., Faraday Trans. 2* **1986**, 82, 41.

(17) Kearley, G. J. *Nucl. Instrum. Methods Phys. Res. A* **1995**, 354, 53.

(18) van Schilfgarde, M.; Paxton, T. A.; Jespen, O.; Krier, G.; Burkhard, A.; Andersen, O. K. *Program TB-LMTO 4.6*; Max-Planck Institut Stuttgart: Stuttgart, 1994.

(19) von Barth, U.; Hedin, L. *J. Phys. C* **1995**, 5, 1629.

(20) Krier, G.; Andersen, O. K.; Jespen, O. Unpublished.

(21) Jespen, O.; Andersen, O. K. *Z. Phys. B* **1995**, 97, 35.

(22) Jespen, O.; Andersen, O. K. *Solid State Commun.* **1971**, 9, 1763.

(23) Blöchl, P.; Jespen, O.; Andersen, O. K. *Phys. Rev. B* **1994**, 49, 16223.

(14) Kadir, K.; Kritikos, M.; Noréus, D.; Andresen, A. F. *J. Less Common Met.* **1991**, 172–174, 36.

(15) Penfold, J.; Tomkinson, J. *The ISIS Time Focused Crystal Spectrometer, TFXA*; Rutherford Appleton Laboratory: Oxford, U.K., 1986; RAL-86-019.

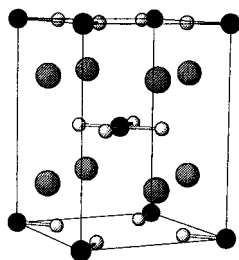


**Figure 1.** The crystallographic structure of  $K_2PdH_4$ , with four hydrogen atoms bonded to each palladium, surrounded by potassium atoms (gray spheres).

**Table 1.** Observed Band and Assignments for  $K_2PdH_4$  in  $D_{4h}$  Symmetry

IR ( $cm^{-1}$ )	Raman ( $cm^{-1}$ )	INS ( $cm^{-1}$ )	assignment
	1810	1840	$\nu(Pd-H)$ $A_{1g}$
	1810	1840	$\nu(Pd-H)$ $B_{2g}$
1500 vs		1520	$\nu(Pd-H)$ $E_u$
		1280	$\delta(H-Pd-H)$ $B_{2u}$
	826	826	$\delta(H-Pd-H)$ $B_{1g}$
800 m		820	$\delta(H-Pd-H)$ $A_{2u}$
800 m		820	$\delta(H-Pd-H)$ $E_u$
		480	libration ( $R_z$ ) $A_{2g}$
		430	libration ( $R_x, R_y$ ) $E_u$

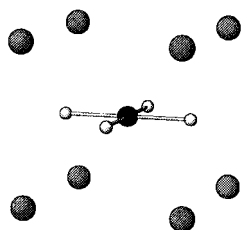


**Figure 2.** The model used in the CLIMAX refinement of  $K_2PdH_4$ . One square planar  $PdH_4$ -complex with  $D_{4h}$  symmetry surrounded by the eight closest potassium atoms.

of-plane deformation ( $A_{2u}$ ) are IR active and the symmetric ( $A_{1g}$ ) and anti-symmetric ( $B_{2g}$ ) stretches and the in-plane deformation ( $B_{1g}$ ) are Raman active. In the mid-IR spectrum only two modes were observed: one at  $1500\text{ cm}^{-1}$  and one at  $800\text{ cm}^{-1}$ . The Raman spectrum also showed two modes one at  $1810\text{ cm}^{-1}$  and one at  $826\text{ cm}^{-1}$ . The INS spectrum shows that all deformations, except one at  $1280\text{ cm}^{-1}$ , are accidentally degenerate at  $820\text{ cm}^{-1}$ , which explains why only two peaks are observed in the IR spectra. The proposed assignment of the INS spectrum of  $K_2PdH_4$  is shown in Table 1, which also closely corresponds to recent Raman data on the structural analogue  $K_2PtH_4$ .<sup>24</sup> The model used for describing the normal vibrations of the square-planar  $PdH_4$  is shown in Figure 2, which corresponds exactly to the local environment around the complexes in the crystal. The potassium atoms were included in the model to generate the libration modes. The CLIMAX input files contain 13 atoms and 26 internal coordinates (4 Pd–H stretches, 16 K–H stretches, 4 Pd–H bends, and 2 Pd–H linear angle bends) and 16 symmetry coordinates. Four fundamental and five interaction constants were used to fit the calculated to the observed INS data. The resulting fit is shown in Figure 3 and the calculated force constants in Table 2.

**$Li_2PdH_2$  and  $Na_2PdH_2$**  are isostructural and crystallize in the tetragonal space group  $I4/mmm$  with unit cell dimensions  $a = 3.111(1)\text{ \AA}$ ,  $c = 10.333(2)\text{ \AA}$  (Li) and  $a = 3.599(1)\text{ \AA}$ ,  $c = 11.327(3)\text{ \AA}$  (Na). As shown in Figure 4 both hydrides consist

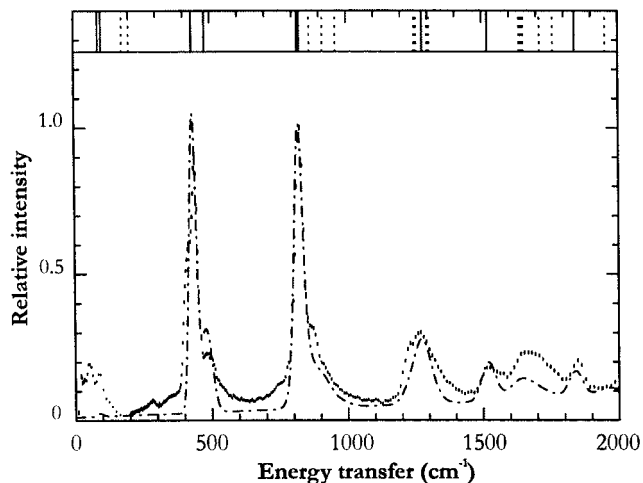


**Figure 3.** The observed and calculated INS spectra of  $K_2PdH_4$ . Above the spectra the fundamental vibrations (filled lines), combinations bands, and first overtones (dotted lines) are marked.

**Table 2.** Force Constants of  $K_2PdH_4$  in  $D_{4h}$  Symmetry

force constants <sup>a</sup>		description
$F_1$	1.66	Pd–H stretch
$i_1$	0.34	Pd–H/Pd–H stretch interaction
$F_2$	0.15	K–H stretch (defines the librations)
$i_2'$	0.085	$R_z/R_z$ interaction
$i_2''$	–0.0068	$(R_x, R_y)/(R_x, R_y)$ interaction
$F_3$	0.51	$PdH_2$ in-plane deformation
$i_3$	0.12	$PdH_2/PdH_2$ in-plane def. interaction
$F_4$	0.820	$PdH_2$ out-of-plane deformation
$i_4$	–0.45	$PdH_2/PdH_2$ out-of-plane def. interaction

<sup>a</sup> Fundamental force constants ( $F$ ) are in  $mdyn/\text{\AA}$  and the interaction force constants ( $i$ ) are in  $mdyn/\text{\AA}^2$ .



**Figure 4.** The crystallographic structure of  $A_2PdH_2$  ( $A = Li$  or  $Na$ ). In the structure two hydrogen atoms (white spheres) are bonded to one palladium surrounded by lithium or sodium atoms (gray spheres).

of linear ( $D_{\infty h}$ ), anionic  $PdH_2$  complexes surrounded by lithium or sodium counterions in a bicapped cubic configuration. The Pd–H distances are equal within one standard deviation at  $1.68\text{ \AA}$ . The shortest Li–H distance is  $2.03\text{ \AA}$  and the corresponding Na–H distance is  $2.42\text{ \AA}$ . The shortest distances between the hydrogens on adjacent complexes are  $2.85$  (Li) and  $3.43\text{ \AA}$  (Na).

The INS spectra of  $Li_2PdH_2$  (Figure 5) and  $Na_2PdH_2$  are similar except that the  $Li_2PdH_2$  spectrum is shifted to higher energy. They both show interesting features as dispersion of libration and bending modes and there is also an onset of a continuum of scattering density above  $\sim 1000\text{ cm}^{-1}$  in both spectra. This is probably caused by atomic recoil, which often occurs for light atoms in shallow wells. The continuum was estimated mathematically and extracted from the data used in the CLIMAX refinements.

(24) Suchanek, E.; Lange, N.; Auffermann, G.; Bronger, W.; Lutz, H. *J. Raman Spectrosc.* **1999**, *30*, 981.

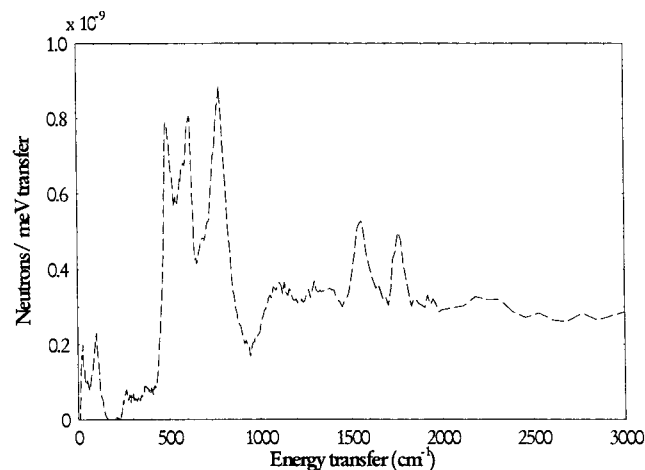


**Figure 5.** The raw INS spectrum of  $\text{Li}_2\text{PdH}_2$ . The dispersion of the libration ( $\sim 600\text{ cm}^{-1}$ ) and bending ( $\sim 800\text{ cm}^{-1}$ ) modes and the increase in background intensity (between 800 and 1100  $\text{cm}^{-1}$ ) are clearly seen.

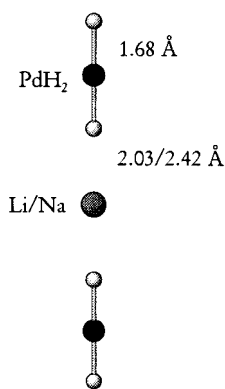


**Figure 6.** The model used in the CLIMAX refinement of  $\text{A}_2\text{PdH}_2$  ( $\text{A} = \text{Li}$  or  $\text{Na}$ ). Two linear  $\text{PdH}_2$ -complexes, with one  $\text{A}$  atom between, were used to generate the dispersion, in accordance with  $D_{\infty h}$  symmetry.

The model used in the CLIMAX refinements is shown in Figure 6. One alkali metal ( $\text{A}$ ) and two  $\text{PdH}_2$ -molecules were included to describe the libration by using  $\text{H-Pd-A}$  linear angle bends and to approximate the dispersion of the libration and deformation modes. To reduce the number of internal coordinates only one alkali metal, placed between the complexes, was included. In a more complete model also the interaction in the crystallographic  $ab$  plane must be included. The CLIMAX input files contain 7 atoms and 12 internal coordinates (4  $\text{Pd-H}$  stretches, 4  $\text{H-Pd-H}$  linear angle bends, and 4  $\text{H-Pd-A}$  linear angle bends) and 12 symmetry coordinates.  $\text{Li}_2\text{PdH}_2$  and  $\text{Na}_2\text{PdH}_2$  both show metallic character in their conductivity and luster. Because of the high reflectivity IR or Raman spectroscopy could not be used to identify the character of the peaks in the INS spectra.

The assignment of the bands in the spectra was suggested by comparing the  $\text{PdH}_2\text{-A-PdH}_2$  unit with the square-planar  $\text{PdH}_4$ -complex found in  $\text{K}_2\text{PdH}_4$ . The IR and Raman data for  $\text{K}_2\text{PdH}_4$  show that the double degenerated anti-symmetric stretch ( $E_u$ ) lies lower in energy than both the symmetric stretch ( $A_{1g}$ ) and the anti-symmetric stretch ( $B_{2g}$ ). If the square-planar complex is divided into two linear complexes and the stretches are separated accordingly, the symmetric in- and out-of-phase modes of the  $\text{PdH}_2\text{-A-PdH}_2$  unit are obtained from the symmetric ( $A_{1g}$ ) and the anti-symmetric ( $B_{2g}$ ) stretches of  $\text{PdH}_4$ . The anti-symmetric in- and out-of-phase  $\text{PdH}_2\text{-A-PdH}_2$  stretches are obtained from the double degenerated stretch ( $E_u$ ) of  $\text{PdH}_4$  (Figure 7). We believe this is a strong argument for assigning

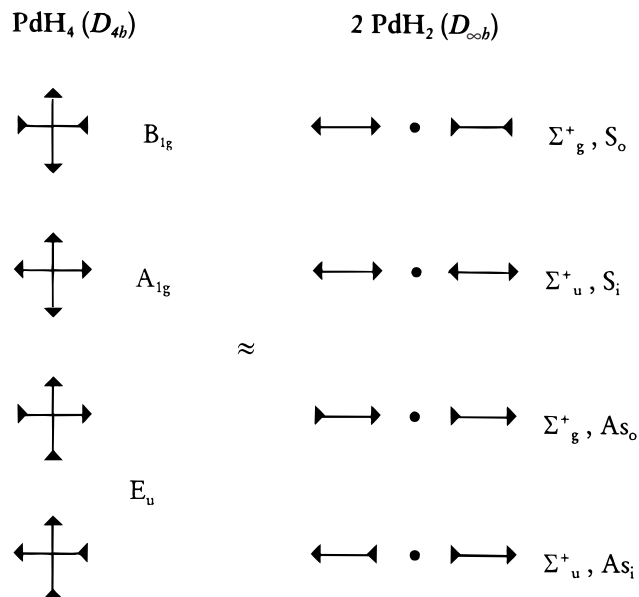


**Figure 7.** The relation between the stretches of  $\text{PdH}_4$  in  $D_{4h}$  symmetry and the stretches of the two coupled  $\text{PdH}_2$  in  $D_{\infty h}$  symmetry. “S” denotes a symmetric stretch and “As” an anti-symmetric stretch. “o” denotes out-of-phase and “i” in-phase, in relation to the other  $\text{PdH}_2$  complex.

**Table 3.** Observed Bands and Assignments of the INS Spectra of  $\text{Li}_2\text{PdH}_2$  and  $\text{Na}_2\text{PdH}_2$  in  $D_{4h}$  Symmetry

$\text{Li}_2\text{PdH}_2$ ( $\text{cm}^{-1}$ )	$\text{Na}_2\text{PdH}_2$ ( $\text{cm}^{-1}$ )	assignment
1775	1675	$\nu(\text{Pd-H})$ out-of-phase $\Sigma_u^+$
1755	1645	$\nu(\text{Pd-H})$ in-phase $\Sigma_g^+$
1590	1455	$\nu(\text{Pd-H})$ out-of-phase $\Sigma_u^+$
1550	1425	$\nu(\text{Pd-H})$ in-phase $\Sigma_g^+$
775	750	$\delta(\text{PdH}_2)$ in-phase $\Pi_u$
775	750	$\delta(\text{PdH}_2)$ in-phase $\Pi_u$
730	720	$\delta(\text{PdH}_2)$ out-of-phase $\Pi_g$
730	720	$\delta(\text{PdH}_2)$ out-of-phase $\Pi_g$
590	545	libration ( $R_x, R_y$ ) in-phase $\Pi_u$
590	545	libration ( $R_x, R_y$ ) in-phase $\Pi_u$
500	475	libration ( $R_x, R_y$ ) out-of-phase $\Pi_g$
500	475	libration ( $R_x, R_y$ ) out-of-phase $\Pi_g$

the symmetric stretches to the highest energy. Parker et al. have also shown that this is not an unusual assignment for  $\text{TMH}_4$ -complexes.<sup>25,26</sup> In the assignment and the refinements we assumed that the *ungerade* modes lie higher in energy than the *gerade* modes for our model, since the center of mass is not changed for the latter. The proposed assignment of the INS spectra is shown in Table 3. The previous assignment and CLIMAX refinement on  $\text{Na}_2\text{PdH}_2$  accounted only for the internal modes and proposed that the anti-symmetric stretch was highest in energy, at 2000  $\text{cm}^{-1}$ , but in the present assignment this broad feature is better described as overtones and combination bands.<sup>27</sup> Three fundamental and five interaction constants were used to fit the calculated spectra to the observed spectra. The resulting fits are shown in Figure 8, parts a and b, and the calculated force constants in Table 4.

Our new assignment on  $\text{Na}_2\text{PdH}_2$  is also consistent with the one recently proposed by Liao et al.<sup>7</sup> Here, however, we should note that their calculations on a  $\text{A}_2\text{PdH}_2$  unit in a crystal field are not supported by our experimental results. They expect very similar symmetric stretching frequencies under exchange of Na

(25) Parker, S. F.; Williams, K. P. J.; Bortz, M.; Yvon, K. *Inorg. Chem.* **1997**, *36*, 5218.

(26) Parker, S. F.; Jayasooriya, U. A.; Sprunt, J. C.; Bortz, M.; Yvon, K. *J. Chem. Soc., Faraday Trans.* **1998**, *94*, 2595.

(27) Noréus, D.; Tomkinson, J. *Chem. Phys. Lett.* **1989**, *154*, 439.

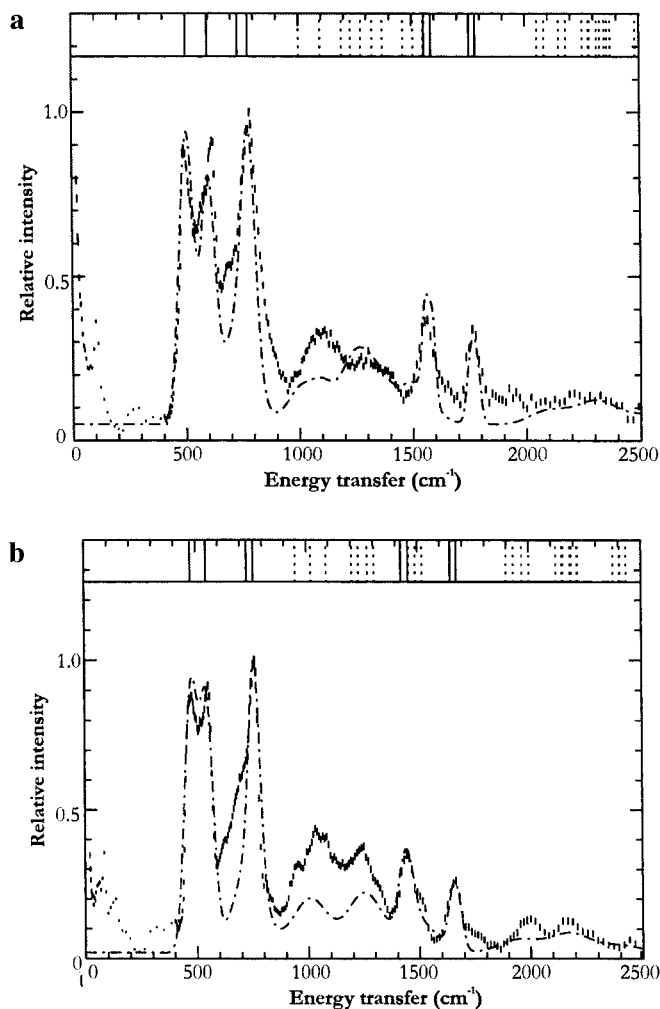


**Figure 8.** (a) The observed and calculated spectra of  $\text{Li}_2\text{PdH}_2$ . (b) The observed and calculated spectra of  $\text{Na}_2\text{PdH}_2$ .

**Table 4.** Force Constants of  $\text{Li}_2\text{PdH}_2$  and  $\text{Na}_2\text{PdH}_2$  in  $D_{4h}$  Symmetry

	force constants <sup>a</sup>		description
	$\text{Li}_2\text{PdH}_2$	$\text{Na}_2\text{PdH}_2$	
$F_1$	1.64	1.42	Pd–H stretch
$i_1$	0.21	0.21	Pd–H/Pd–H str. intra complex interaction
$i_1'$	–0.028	–0.027	Pd–H/Pd–H str. inter complex interaction
$F_2$	0.70	0.69	$\text{PdH}_2$ deformation
$i_2$	0.26	0.28	$\text{PdH}_2/\text{PdH}_2$ def. intra complex interaction
$i_2'$	–0.0003	–0.0004	$\text{PdH}_2/\text{PdH}_2$ def. inter complex interaction
$F_3$	0.29	0.30	Pd–H–M deformation
$i_3$	0.033	0.031	Pd–H–M/Pd–H–M def. interaction

<sup>a</sup> Fundamental force constants ( $F$ ) are in  $\text{mdyn}/\text{\AA}$  and interaction constants ( $i$ ) are in  $\text{mdyn}/\text{\AA}^2$ .

for Li. In our INS studies the vibrational frequency assigned as the symmetric stretch of  $\text{Li}_2\text{PdH}_2$  was found  $100\text{ cm}^{-1}$  higher in energy than the corresponding symmetric stretch of  $\text{Na}_2\text{PdH}_2$  and the difference in the fundamental stretching force constants was 15%. It should be remembered, however, that our division of the force constant contribution to the observed hydrogen vibration frequencies is model dependent. In the Li compound the hydrogen is more firmly bound to the lattice, but with our applied simple model it may be premature to almost entirely assign the difference to the Pd–H bonds in the two hydrides.

$\text{NaBaPdH}_3$  crystallizes in the hexagonal space group  $P6_3/mmc$  (No. 194) with the unit cell dimensions  $a = 6.0611(6)\text{ \AA}$  and  $c = 6.0859(8)\text{ \AA}$  at room temperature. In the structure

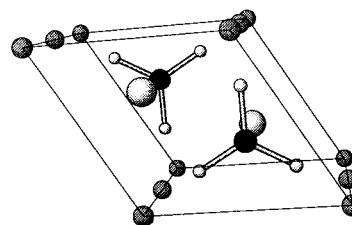


**Figure 9.** The hexagonal unit cell of  $\text{NaBaPdH}_3$ . The  $\text{PdH}_3$ -complexes are surrounded by Ba (large white spheres) and sodium (small gray spheres).

**Table 5.** Observed Bands and Assignments of the INS Spectra of  $\text{NaBaPdH}_3$

IR ( $\text{cm}^{-1}$ )	INS ( $\text{cm}^{-1}$ )	assignment
1400	1410	anti symmetric Pd–H stretch $E'$
1400	1410	anti symmetric Pd–H stretch $E'$
	1370	symmetric $\text{PdH}_3$ stretch $A'_1$
	620	out-of-plane deformation $A''_2$
	470	in-plane deformation $E'$
	470	in-plane deformation $E'$
	410	libration ( $R_x, R_y$ ) $E'$
	410	libration ( $R_x, R_y$ ) $E'$
	361	libration ( $R_z$ ) $A'_2$

(Figure 9) trigonal planar ( $D_{3h}$ )  $\text{PdH}_3$ -complexes are counterbalanced by sodium and barium atoms. The Pd–H distance of  $1.72\text{ \AA}$  is somewhat longer than in the previous zerovalent complexes indicating a weaker bond. The Na–H distance of  $2.33\text{ \AA}$  is remarkably short compared with the Na–H distances found in  $\text{NaH}$  and  $\text{Na}_2\text{PdH}_2$ , thus indicating a stronger interaction between the hydrogens and the cations. The Ba–H distance is longer than the shortest distances found in  $\text{BaH}_2$  and we expect a correspondingly small interaction between barium and hydrogen in  $\text{NaBaPdH}_3$ , and therefore we excluded the barium atoms in the CLIMAX model.

When comparing the INS spectra of  $\text{K}_2\text{PdH}_4$ ,  $\text{Li}_2\text{PdH}_2$ , and  $\text{Na}_2\text{PdH}_2$  with the spectra of  $\text{NaBaPdH}_3$ , the latter differ by being shifted to lower energy with the highest stretching mode around  $1400\text{ cm}^{-1}$ , indicating a slightly more “hydrogen-in-metal” like system compared with the compounds discussed earlier. This can be compared to a Pd–H vibration of about  $2040\text{ cm}^{-1}$  for gaseous Pd–H and vibrational modes centered about  $450\text{ cm}^{-1}$  in the solid PdH metal hydride.<sup>28,29</sup> An IR recording of  $\text{NaBaPdH}_3$  showed only a weak, but sharp feature at  $1400\text{ cm}^{-1}$ , and from the selection rules for IR spectra in  $D_{3h}$  symmetry, this was assigned as the double degenerated anti-symmetric stretch ( $E_u$ ). The proposed assignment scheme is shown in Table 5.

A sloping background and the intensity of the second overtones and combination bands were extracted from the raw data before force field refinements by CLIMAX.

The CLIMAX model consists of one  $\text{PdH}_3$  complex and the six adjacent sodium atoms (Figure 10). The symmetry ( $D_{3h}$ ) and the distances obtained from the crystallographic investigation were used. The model differs from that described earlier by the need to incorporate the influence of the counterions more thoroughly. The sodium atoms were used to generate not only the external modes, but also internal modes by using three coupled  $\text{Na}_2$ –Pd–H units instead of a  $\text{PdH}_3$  unit surrounded by six sodium atoms. For example, the  $\text{PdH}_3$  in-plane deforma-

(28) Estimated from the measured Pd–D frequency of  $1446\text{ cm}^{-1}$ . (a) Malmberg, C.; Shullman, R.; Nylén, P. *Ark. Fys.* **1969**, *39*, 495. (b) Rohlfling, C. M.; Hay, P. J.; Martin, R. L. *J. Chem. Phys.* **1986**, *85*, 1447.

(29) Ross, D. K.; Antonov, V. E.; Bokhenov, E. L.; Kolesnikov, A. I.; Ponyatovsky, E. G.; Tomkinson, J. *Phys. Rev. B* **1998**, *58*, 2591.

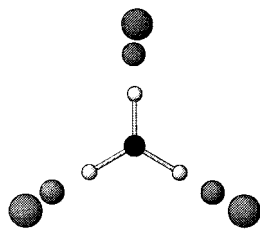


**Figure 10.** The model used in the CLIMAX refinement. One trigonal planar PdH<sub>3</sub>-complex and the six closest sodium atoms were included in accordance with *D*<sub>3h</sub> symmetry.

**Table 6.** Force Constants of NaBaPdH<sub>3</sub> in *D*<sub>3h</sub> Symmetry

force constants		description
<i>F</i> <sub>1</sub>	0.91	Pd-H stretch
<i>i</i> <sub>1</sub>	-0.0094	Pd-H/Pd-H str. interaction
<i>F</i> <sub>2</sub>	0.096	Na-H stretch
<i>i</i> <sub>2</sub>	-0.0078	Na-H/Na-H str. interaction
<i>F</i> <sub>3</sub>	0.41	Na-H-Na bend
<i>F</i> <sub>4</sub>	0.054	Pd-H-Na <sub>2</sub> out-of-plane def.
<i>i</i> <sub>4</sub>	0.011	Pd-H-Na <sub>2</sub> out-of-plane def. interaction
<i>F</i> <sub>5</sub>	0.42	Na-H-Na bend

<sup>a</sup> Fundamental force constants (*F*) are in mdyn/Å and interaction constants (*i*) are in mdyn/Å<sup>2</sup>.

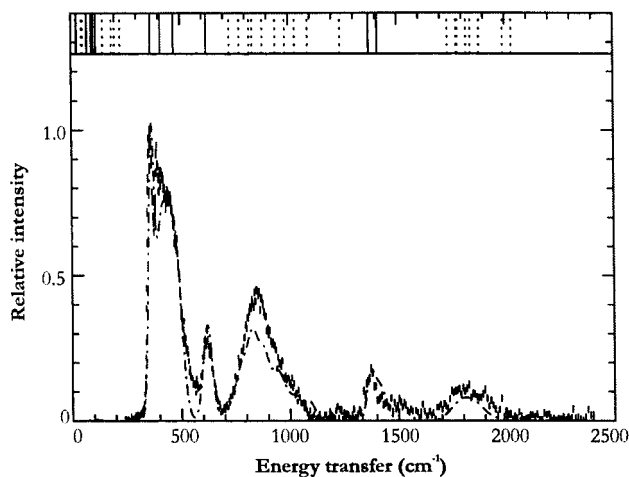


**Figure 11.** The observed and calculated spectra of NaBaPdH<sub>3</sub>.

tions were generated by Na<sub>2</sub>-Pd-H out-of-plane deformations instead of PdH<sub>2</sub> bends. To describe the internal and external modes 21 internal coordinates (3 Pd-H stretches, 6 Na-H stretches, 6 Pd-H-Na bends, 3 Na-H-Na bends, and 3 Pd-H-Na<sub>2</sub> out-of-plane deformations) were used. In the CLIMAX refinement 5 fundamental and 3 interaction force constants were used and the obtained force constants are shown in Table 6 and the observed and calculated spectra are shown in Figure 1.

**Ba<sub>2</sub>PdH<sub>4</sub>** crystallizes in the orthorhombic space group *Pnma* (No. 62) with the unit cell dimensions *a* = 7.986(2) Å, *b* = 5.758(2) Å, and *c* = 10.153(4) Å at 150 K. In the structure flattened, distorted PdH<sub>4</sub> tetrahedra were found with Pd-H distances ranging from 1.76 to 1.81 Å, with an average of 1.80 Å. The tetrahedral angles ranged from 105.6° to 121.7° compared with the ideal value of 109.5°. The [PdH<sub>4</sub>]<sup>4-</sup> complexes are counterbalanced by barium ions surrounding each complex in a distorted tricapped cubic configuration, with the capped barium atoms closest to the hydrogen atoms (Figure 12). The structure can also be regarded as being close to an interstitial hydride, with hydrogen in octahedral holes formed by one Pd and five Ba atoms.

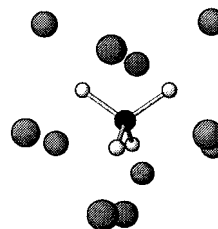


**Figure 12.** The Ba coordination around one flattened tetrahedral PdH<sub>4</sub>-complex in the structure of Ba<sub>2</sub>PdH<sub>4</sub>.

**Table 7.** Observed Bands and Assignment of the INS Spectra of Ba<sub>2</sub>PdH<sub>4</sub>

INS (cm <sup>-1</sup> )	assignment	INS (cm <sup>-1</sup> )	assignment
1290	Pd-H stretch A <sub>1</sub>	572	PdH <sub>4</sub> deformation B <sub>1</sub>
1200	Pd-H stretch B <sub>2</sub>	527	PdH <sub>4</sub> deformation E
1080	Pd-H stretch E	527	PdH <sub>4</sub> deformation E
1080	Pd-H stretch E	515	libration A <sub>2</sub>
620	PdH <sub>4</sub> deformation A <sub>1</sub>	420	libration E
590	PdH <sub>4</sub> deformation B <sub>2</sub>	420	libration E

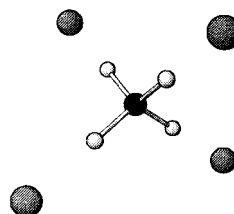


**Figure 13.** The model used in the CLIMAX refinement of Ba<sub>2</sub>PdH<sub>4</sub>. The flattened tetrahedron was described using *D*<sub>2d</sub> symmetry and four barium atoms (gray spheres) representing the lattice were placed in a straight line from each hydrogen atom.

The hydride crystallizes in dark brown irregular crystals and a resistivity measurement on a powdered sample at room temperature shows that Ba<sub>2</sub>PdH<sub>4</sub> is nonconducting.<sup>11</sup> Unfortunately no IR or Raman spectra could be recorded.

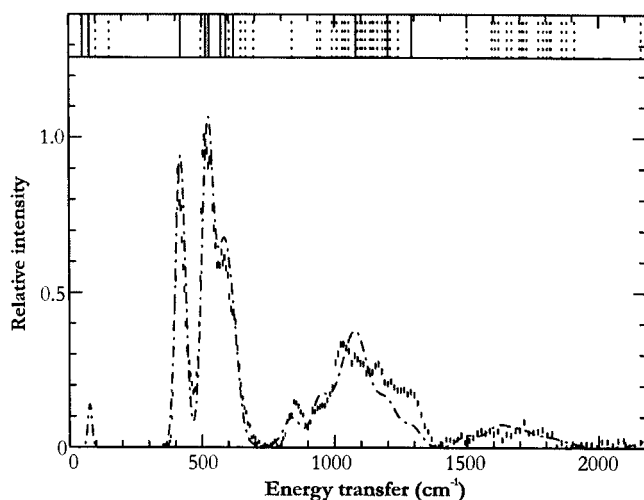
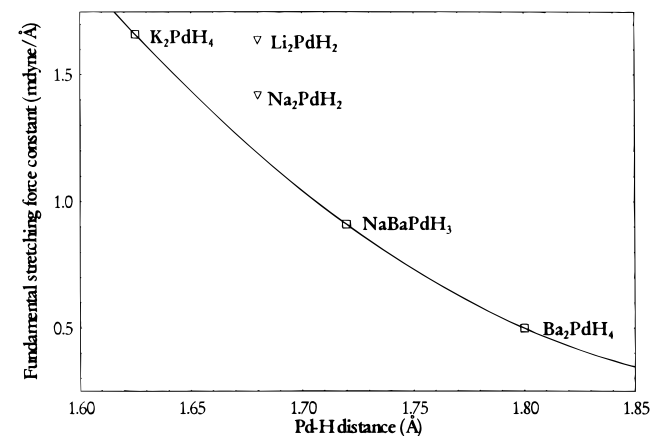
The INS spectra is similar to that of NaBaPdH<sub>3</sub>, but shifted even further to lower energy. The largest intensity is found in the region between 400 and 700 cm<sup>-1</sup>, with a broad band between 800 and 1380 cm<sup>-1</sup>. Integrating the bands suggested the presence of 8 modes in the lower region, which we assigned as the librations and deformations. The proposed assignment is shown in Table 7. This assignment gave a rather good fit. Even if the details remain uncertain, especially in the lower region, the ambiguities, however, will not affect the estimates for the force constants too much. The fit supports a picture in agreement with that given for the complexes above: a molecular-like palladium complex but with substantial support from the cations.

The symmetry used in the CLIMAX model was *D*<sub>2d</sub>, corresponding to a flattened *T*<sub>d</sub>-geometry. The angles were set to 115° and 106°, with an average Pd-H distance of 1.80 Å. Four Ba atoms were placed in line with the Pd-H directions at a distance of 2.75 Å from the hydrogen atoms, which represents the average distance of the closest Ba-H contacts (Figure 13).

In the CLIMAX model we used 9 atoms in the model (1 Pd, 4 H, and 4 Ba) and 18 internal coordinates (4 Pd-H stretches, 4 Ba-H stretches, 6 H-Pd-H bonds, and 12 Ba-Ba-Pd-H torsions) were generated. The torsions were used to describe the librations and the Ba-H stretches to describe the translations. In the CLIMAX refinement four fundamental force constants and seven interaction force constants were refined and the results are shown in Table 8 and the observed and calculated spectra in Figure 14.

**Table 8.** Force Constants of Ba<sub>2</sub>PdH<sub>4</sub> in D<sub>2d</sub> Symmetry

force constants		description
$F_1$	0.50	Pd–H stretch
$i_1'$	0.12	PdH/PdH str. interaction (115°)
$i_1''$	0.033	PdH/PdH str. interaction (106°)
$F_2$	0.23	PdH def.
$i_2'$	-0.095	PdH/PdH def. interaction (115°)
$i_2''$	-0.029	PdH/PdH def. interaction (106°)
$i_2'''$	-0.038	PdH/PdH def. interaction (106°)
$F_3$	0.30	Ba–H stretch
$F_4$	0.35	Pd–H–Ba <sub>2</sub> torsion
$i_4'$	-0.30	Pd–H–Ba <sub>2</sub> /Pd–H–Ba <sub>2</sub> torsion interaction
$i_4''$	-0.50	Pd–H–Ba <sub>2</sub> /Pd–H–Ba <sub>2</sub> torsion interaction

**Figure 14.** The observed and calculated spectra of Ba<sub>2</sub>PdH<sub>4</sub>.**Figure 15.** The fundamental stretching force constants obtained from the CLIMAX refinement versus the Pd–H distances obtained from the crystallographic investigations.

**Bonding in the Molecular Entities.** A substantial decreasing bond strength is seen in Figure 15 for the trigonal and tetragonal complexes as expressed in increasing bond length and decreasing fundamental stretching force constant. The curve is just a guide to the eye but shows a  $1/d_{\text{Pd-H}}$  behavior of the force constant. How can the general trends in Figure 15 be explained in terms of electronic structure or hybridizations of the complexes and their interaction with the cations in the surrounding lattice? So far our results point to a predominantly molecular description of the complexes. For reasons that will become clearer later we will start with a simple group theoretical consideration of the hydrido complexes on the basis of bonding inactive Pd 5p orbitals, according to the suggestions by Firman and Landis.<sup>3</sup>

For the PdH<sub>2</sub><sup>2-</sup> entity the central atom basis function

transform as  $\Sigma_g$  (5s, 4d<sub>z<sup>2</sup></sub>),  $\Pi_g$  (4d<sub>xz</sub>, 4d<sub>yz</sub>), and  $\Delta_g$  (4d<sub>x<sup>2</sup>-y<sup>2</sup></sub>, 4d<sub>xy</sub>), whereas the ligand orbitals supply combinations with  $\Sigma_g$  and  $\Sigma_u$  symmetry. Just the three basis functions with  $\Sigma_g$  symmetry account for Pd–H interaction, yielding a bonding, a nonbonding (corresponds basically to the Pd 5s orbital), and an antibonding MO (Figure 16a). The bond order, BO, of a Pd–H bond might be defined as

$$\text{BO} = \frac{(N_{\text{bonding}} - N_{\text{antibonding}})}{2L}$$

where  $N_{\text{bonding}}$  and  $N_{\text{antibonding}}$  are the number of bonding and antibonding electrons in the respective MO's and L is the number of ligand species. In the 14-electron complex the bonding and all nonbonding MOs are occupied and the BO is calculated to 1/2. In the complementary VB description of Firman and Landis<sup>3</sup> this bonding picture is expressed by a three-center, four-electron bond with 5 lone pairs organized into a hypervalent PdH<sub>2</sub><sup>2-</sup> entity.

Similarly in PdH<sub>4</sub><sup>2-</sup> the Pd basis functions transform as A<sub>1g</sub> (5s, 4d<sub>z<sup>2</sup></sub>), B<sub>1g</sub> (4d<sub>x<sup>2</sup>-y<sup>2</sup></sub>), B<sub>2g</sub> (4d<sub>xy</sub>), and E<sub>g</sub> (4d<sub>xz</sub>, 4d<sub>yz</sub>), and the ligand orbital combinations as A<sub>1g</sub>, E<sub>u</sub>, and B<sub>1g</sub>. The resulting diagram for the occupied MO's (2 bonding and 6 nonbonding) for a 16-electron complex are shown in Figure 16b. As in PdH<sub>2</sub><sup>2-</sup> the bond order for a Pd–H bond is 1/2 and in the VB description this situation corresponds to two three-center, four-electron bonds and 4 lone pairs.<sup>3</sup>

For the electron-rich Pd(0) complexes PdH<sub>3</sub><sup>3-</sup> and PdH<sub>4</sub><sup>4-</sup> we obtain a situation where Pd–H antibonding MO's have to be occupied (Figure 16, c and d). This reduces the bond order for a Pd–H bond to 1/3 in the 16-electron entity PdH<sub>3</sub><sup>3-</sup> and 1/4 in the 18-electron species PdH<sub>4</sub><sup>4-</sup>. Qualitatively the bond strength expressed as stretching force constant scales well with the obtained BO in these simple MO considerations.

With the inclusion of Pd 5p orbitals as basis functions it would be possible to obtain for all four entities PdH<sub>2</sub><sup>2-</sup>, PdH<sub>4</sub><sup>2-</sup>, PdH<sub>3</sub><sup>3-</sup>, and PdH<sub>4</sub><sup>4-</sup> a bonding situation with two-center, two electron bonded ligands (model of Bayse and Hall<sup>5</sup>). However, the experimental results contradict this bonding description when looking at the trends in Pd–H distances and stretching force constants as shown in Figure 15. The electron-rich complexes PdH<sub>3</sub><sup>3-</sup> and PdH<sub>4</sub><sup>4-</sup> do not, however, fit the description of Landis and Firman either. Rather they emphasize that hydrido complexes with delocalizations greater than 3c-4e bonding (as have to be postulated for PdH<sub>3</sub><sup>3-</sup> and PdH<sub>4</sub><sup>4-</sup>) are unstable and lose hydride ligands to the interstitial positions in the counteratom framework. The obvious existence of trigonal planar Pd<sup>0</sup>H<sub>3</sub><sup>3-</sup> and flattened tetrahedral Pd<sup>0</sup>H<sub>4</sub><sup>4-</sup> in solid-state hydrides demonstrates the significance of the surrounding cationic matrix for the stability of these hydrido complexes. Increasing counterion interaction with the molecular entities is underlined by the increasing band broadening in the vibrational spectra in the order K<sub>2</sub>PdH<sub>4</sub> → Na<sub>2</sub>PdH<sub>2</sub> → Li<sub>2</sub>PdH<sub>2</sub> → NaBaPdH<sub>3</sub> → Ba<sub>2</sub>PdH<sub>4</sub>. A strong counterion influence was also suggested by Liao et al. in their recent theoretical investigation of the molecular units Li<sub>2</sub>PdH<sub>2</sub> and Na<sub>2</sub>PdH<sub>2</sub>.<sup>7</sup> When the effect of the crystal field was included, they observed an increase of the Pd–H distance of ca. 0.05 Å.

**Bonding in the Solid-State Compounds.** Figure 17 summarizes the band structures in the solid-state Pd hydrides Na<sub>2</sub>PdH<sub>4</sub>, Na<sub>2</sub>PdH<sub>2</sub>, Li<sub>2</sub>PdH<sub>2</sub>, NaBaPdH<sub>3</sub>, and Ba<sub>2</sub>PdH<sub>4</sub>. In the left-hand panel the relationship of the bands to the MOs of the molecular entities is indicated, whereas in the right-hand panel the contribution of the cation matrix to the valence band is displayed in a so-called fat-band representation.<sup>21</sup> Consistent

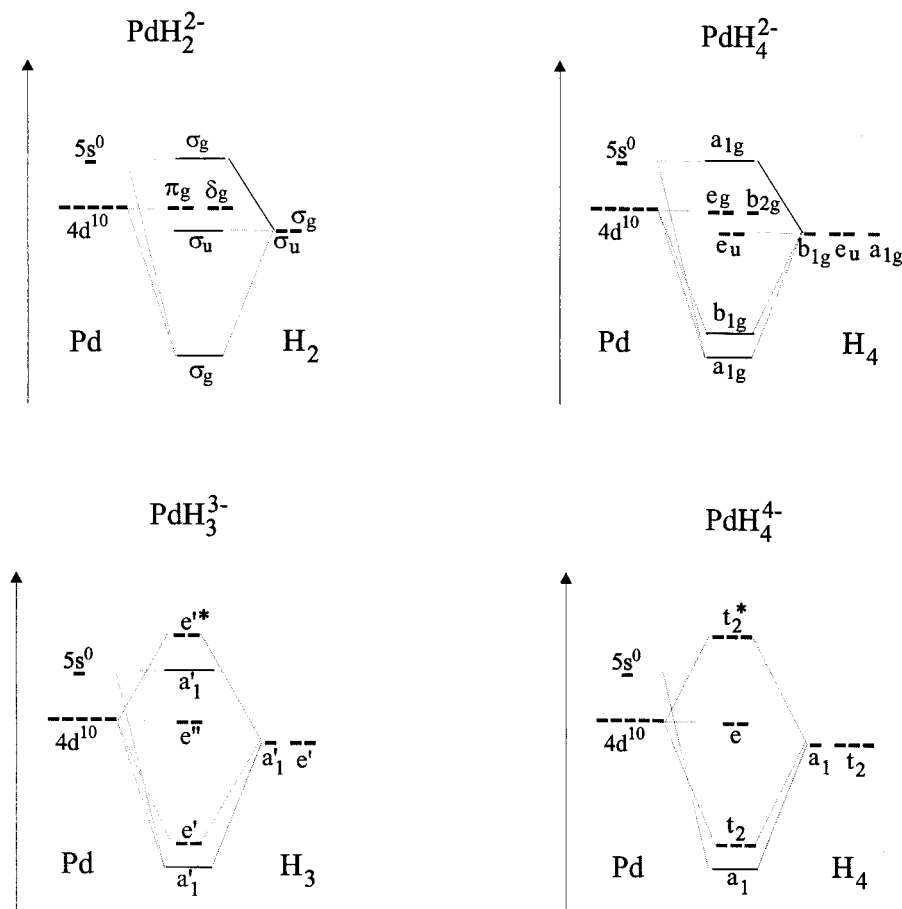


**Figure 16.** Approximate MO diagrams for (a) PdH<sub>2</sub><sup>2-</sup>, (b) PdH<sub>4</sub><sup>2-</sup>, (c) PdH<sub>3</sub><sup>3-</sup>, and (d) PdH<sub>4</sub><sup>4-</sup>. Only occupied MOs are shown. For simplicity the energy of the nonbonding MOs is not changed with respect to the corresponding atomic energy levels.

with the ideas of Firman and Landis we found only a minimal contribution of the Pd 5p orbital to the valence bands.

**Na<sub>2</sub>PdH<sub>4</sub>:** In the band structure of Na<sub>2</sub>PdH<sub>4</sub> the MO diagram for PdH<sub>4</sub><sup>2-</sup> (Figure 17a) is easily recognized. A band gap of ≈1.2 eV separates the conduction band from the six bands corresponding to the nonbonding occupied MOs. The two lowest lying bands (between -8 and -9.5 eV) coincide with the Pd–H bonding MOs. Although Na<sub>2</sub>PdH<sub>4</sub> may appear as a salt-like compound with discrete 16-electron PdH<sub>4</sub><sup>2-</sup> entities, considerable Na–H interaction is present. This is indicated in the dispersed lowest lying Pd–H bonding and the H-based nonbonding (e<sub>u</sub>) bands with large Na contribution.

**Na<sub>2</sub>PdH<sub>2</sub> and Li<sub>2</sub>PdH<sub>2</sub>:** For the Pd hydrides with linear complexes the PdH<sub>2</sub><sup>2-</sup> MO diagram is rather camouflaged in the band structures (Figure 17b,c). This is first due to the large alkaline metal–H interaction, which is more pronounced in Li<sub>2</sub>PdH<sub>2</sub>. The 1σ<sub>g</sub> and σ<sub>u</sub> based bands with the highest H contribution are most affected and largely dispersed, especially along the direction Γ–Z (compare with Na<sub>2</sub>PdH<sub>4</sub>, Figure 17a). Second, there is a huge dispersion (of ≈4 eV) of the bands stemming from the nonbonding MO 2σ<sub>g</sub> along the direction Γ–X, which is accompanied by an avoided crossing with the π<sub>g</sub> based bands. This phenomena appears as a consequence of the interaction of the linear hydrido units within the crystallographic *ab*-plane (distance 3.6 Å) and pushes the 2σ band above the Fermi level (in the direction X–P) which makes the two compounds Na<sub>2</sub>PdH<sub>2</sub> and Li<sub>2</sub>PdH<sub>2</sub> become metallic conductors. Chemically this corresponds to a transfer of a small number of electrons from the hydrido complex units to the alkaline metal matrix. The nature of the metallic conductivity of Na<sub>2</sub>PdH<sub>2</sub> and

Li<sub>2</sub>PdH<sub>2</sub> has been investigated earlier by Kasowski et al. by band structure calculations,<sup>30</sup> but in their work it was not revealed that the actual origin of the conductivity is an intermolecular interaction between the linear PdH<sub>2</sub><sup>2-</sup> entities, i.e., the interaction of the 2σ<sub>g</sub> MOs along Γ–X. This interaction is more pronounced in the Li compound. Indeed by assuming that the 2σ<sub>g</sub> MO is slightly antibonding rather than nonbonding, one could explain the somewhat larger Pd–H stretching force constant of Li<sub>2</sub>PdH<sub>2</sub> compared to Na<sub>2</sub>PdH<sub>2</sub>. The larger intermolecular interaction pushes a larger portion of the 2σ<sub>g</sub> based band above the Fermi level.

**NaBaPdH<sub>3</sub> and Ba<sub>2</sub>PdH<sub>4</sub>:** The band structures of the most interesting electron-rich hydrides NaBaPdH<sub>3</sub> and Ba<sub>2</sub>PdH<sub>4</sub> are shown in Figure 17d,e. Both compounds are semiconductors, as expected from the colors (red for NaBaPdH<sub>3</sub> and brown for Ba<sub>2</sub>PdH<sub>4</sub>), but the band gap in NaBaPdH<sub>3</sub> is rather narrow due to a low-lying Na-s band. (Note the very short Na–Na distance of 3.04 Å within the chains of sodium atoms in this structure.) As for the square-planar and (partly) the linear complex compounds the different groups of occupied MOs of the hydrido complexes PdH<sub>3</sub><sup>3-</sup> and PdH<sub>4</sub><sup>4-</sup> are easily discerned in the band structures. Lowest in energy are the blocks of Pd–H bonding based bands (a<sub>1</sub><sup>'</sup>, e<sup>'</sup>, and t<sub>2</sub> respectively), which are followed by the nonbonding MO and antibonding MO based bands. In Ba<sub>2</sub>PdH<sub>4</sub> e nonbonding and t<sub>2</sub><sup>\*</sup> antibonding bands are clearly separated whereas in NaBaPdH<sub>3</sub> the corresponding bands mix along certain directions. A weaker Pd–H bonding in NaBaPdH<sub>3</sub> and Ba<sub>2</sub>PdH<sub>4</sub> is indicated by the fact that the center of the Pd–H

(30) Kasowski, R. V.; Noréus, D.; Wang, L.; Whangbo, M.-H. *Inorg. Chem.* **1992**, *31*, 4737.



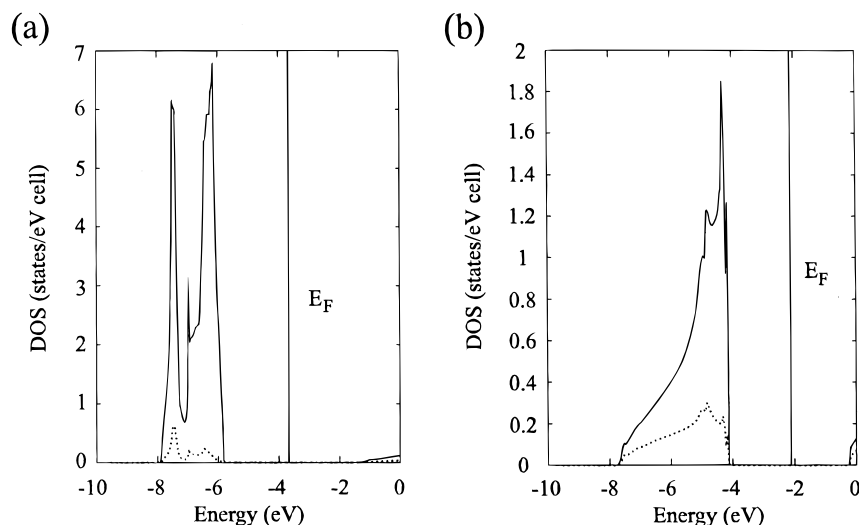


Figure 18. Density of states (DOS) for (a) NaCl and (b) NaH. The Na contribution is indicated by the broken lines.

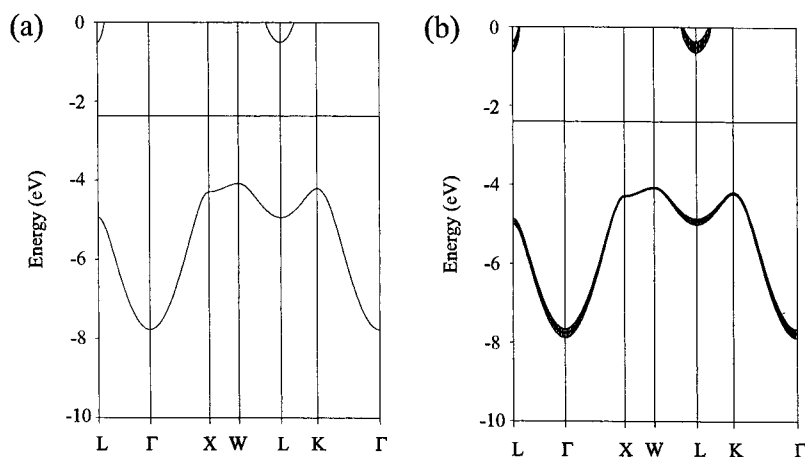


Figure 19. Conventional band structures (a) and band structures with Na contribution in the fat-band representation (b) for NaH.

Na s band giving rise to a considerable dispersion of the valence band (Figures 18b and 19). This reflects the large polarizability of the  $\text{H}^-$  ion and reveals a considerable covalent Na–H bonding contribution even in this ionic hydride.

Hydride structures are often compared with halides, mainly fluorides.<sup>31</sup> As shown here, however, some caution must be considered not to take this analogy too far. Hydrogen is unique with its low electron affinity from filling the K shell. This differentiates hydrides from other compounds, e.g. oxides or halides, where the energy gain from filling a conventional octet more strongly localizes the electrons. Although the radii of  $\text{F}^-$  and  $\text{H}^-$  are similar, there are only two electrons in the latter. Both affects contribute to the large polarizability and the unique softness of  $\text{H}^-$ , leading to what Pearson expresses as a very low resistance to the deformation of the electron density.<sup>32,33</sup>

## Conclusions

The stabilization of four palladium–hydrido complexes, a square-planar  $[\text{Pd}(\text{II})\text{H}_4]^{2-}$ , a linear  $[\text{Pd}(\text{0})\text{H}_2]^{2-}$ , a trigonal  $[\text{Pd}(\text{0})\text{H}_3]^{3-}$  and a slightly distorted  $[\text{Pd}(\text{0})\text{H}_4]^{4-}$ , in the solid-state hydrides  $\text{K}_2[\text{Pd}(\text{II})\text{H}_4]$ ,  $\text{Li}_2[\text{Pd}(\text{0})\text{H}_2]$ ,  $\text{Na}_2[\text{Pd}(\text{0})\text{H}_2]$ ,  $\text{NaBa}[\text{Pd}(\text{0})\text{H}_3]$ , and  $\text{Ba}_2[\text{Pd}(\text{0})\text{H}_4]$  has been studied by investigating the palladium–hydrogen bond strength with inelastic

neutron scattering and by performing self-consistent linear muffin-tin orbital calculations on the corresponding solid-state structures.

The stability, and for the latter two complexes also their existence, could be ascribed to bonding between the hydrogen atoms of the complexes and the cations surrounding the complexes. Such a bonding with substantial covalent contribution between hydrogen and the counterions would also nicely explain the large influence upon the vibrational modes from the distance to the counterions observed for the octahedral complexes in the solid-state hydrides  $\text{A}_2\text{TMH}_6$ , where  $\text{A} = \text{Mg}, \text{Ca}, \text{Sr}, \text{Ba}$  and  $\text{TM} = \text{Ru}, \text{Os}$ .<sup>34</sup> This sensitivity of the strength of the TM–H bonds toward intermolecular interaction was recently commented upon also for a series of hydrides based on platinum–hydrido complexes.<sup>24</sup> The bonding can in a sense be compared with the conventional stabilization of electron-dense formal low oxidation states of the central atom by distributing electron density to suitable ligand orbitals. In homoleptic hydrido complexes where these orbitals are absent, the large polarizability of hydrogen, i.e., the low resistance to a deformation of its electron density, can substitute for this by distributing electron density away from the central atom. This may not have been fully appreciated earlier, maybe due to conventional models for describing formal oxidation states by simply counting the number of electrons, neglecting the fact

(31) Gingl, F.; Gelato, L.; Yvon, K. *J. Alloys Compd.* **1997**, *253*, 286.

(32) Pearson, R. G. *Inorg. Chem.* **1987**, *27*, 734.

(33) Pearson, R. G. *J. Chem. Educ.* **1987**, *64*, 561.

(34) Kritikos, M.; Noréus, D. *J. Solid State Chem.* **1991**, *93*, 256.

that the real electron population in the valence shell of a transition metal is very like that of its atomic state. It is likely that this small electron accepting capacity (in absolute terms) is enough to stabilize the central atom in what conventionally would correspond to a low formal oxidation state.

Related to this is probably also the answer to the puzzling variety of compositions, transition metal coordinations, and geometries in the now rapidly expanding number of new hydrides based on transition metal–hydrido complexes. Hydrogen can adopt any coordination geometry, since its *s*-orbital is spherical and totally symmetric. The low resistance to deformation of the electron density and low electron affinity, which does not contribute much to localize the electrons, will make hydrogen act as an agent for smoothing out the electron density. This facilitates the creation of new hydrides and hydrido complexes, where the structures and geometries will be more dependent on metal atom properties and stoichiometries, as the series of hydrides in the present investigation is an example of. It will further also promote fluxionality, common in many polyhydride complexes, which in a sense is a dynamic analogy to the ease of which these new polyhydride crystals are formed. See, for example, the recent review by Gusev and Berke.<sup>35</sup>

The capacity of the easily polarizable  $H^-$  ion for redistributing electron density has thus probably a somewhat neglected

importance for complex chemistry in general, but the effect has not been elucidated until work in recent years with homoleptic hydrido complexes.

Finally, for hydrides based on complexes with the lowest formal oxidation state on the transition metal and where the largest interaction with the counterions in the surrounding lattice is needed for stabilization, models with a molecular view may come into difficulty.<sup>3,4</sup> In these “hydrogen in metal” like systems a more complete inclusion of the cation lattice into the theoretical treatment has to be considered. In hydrides where the interactions between neighbors become so large that electrons become itinerant, we might further find new interesting electric phenomena relating conductivity with the crystal lattice modes.

**Acknowledgment.** Dr. Winnie Kagunya and Dr. Stewart Parker at ISIS, Rutherford Appleton Laboratory, U.K. are thanked for assistance during the TFXA experiments. The experiments were supported by the European Union through its Training and Mobility of Researchers (TMR) Programme for large scale facilities. This work has also been financially supported by the Swedish Natural Science Research Council (NFR).

JA994089O

---

(35) Gusev, D. G.; Berke H. *Chem. Ber.* **1996**, *129*, 1143.